

Amplified warming from physiological responses to carbon dioxide reduces the potential of vegetation for climate change mitigation

Mingzhu He¹, Shilong Piao ^{1,2✉}, Chris Huntingford ³, Hao Xu¹, Xuhui Wang ¹, Ana Bastos ⁴, Jiangpeng Cui ¹ & Thomas Gasser⁵

Global warming is increasing due to the ongoing rise in atmospheric greenhouse gases, and has the potential to threaten humans and ecosystems severely. Carbon dioxide, the primary rising greenhouse gas, also enhances vegetation carbon uptake, partially offsetting emissions. The vegetation physiological response to rising carbon dioxide, through partial stomatal closure and leaf area increase, can also amplify global warming, yet this is rarely accounted for in climate mitigation assessments. Using six Earth System Models, we show that vegetation physiological response consistently amplifies warming as carbon dioxide rises, primarily due to stomatal closure-induced evapotranspiration reductions. Importantly, such warming partially offsets cooling through enhanced carbon storage. We also find a stronger warming with higher leaf area and less warming with lower leaf area. Our study shows that the vegetation physiological response to elevated carbon dioxide influences local climate, which may reduce the extent of expected climate benefits offered by terrestrial ecosystems.

¹Sino-French Institute for Earth System Science, College of Urban and Environmental Sciences, Peking University, 100871 Beijing, China. ²Institute of Tibetan Plateau Research, Chinese Academy of Sciences, 100101 Beijing, China. ³UK Centre for Ecology and Hydrology, Wallingford, Oxfordshire OX10 8BB, UK. ⁴Department of Biogeochemical Integration, Max Planck Institute for Biogeochemistry, Jena 07745, Germany. ⁵International Institute for Applied Systems Analysis, Laxenburg A-2361, Austria. ✉email: slpiao@pku.edu.cn

Increasing atmospheric greenhouse gas (GHG) levels, caused by the human burning of fossil fuels and land-cover and land-use change, substantially influence human society and ecosystems¹. As atmospheric carbon dioxide (CO₂) concentration (the dominant changing GHG) rises, it enhances carbon sequestration^{2,3}, and currently offsets about 30% of CO₂ emissions⁴. The increased carbon removed by vegetation results in complex land biogeochemical cycling (BGC) changes, many of which further affect climate⁵. In addition to the BGC effects, ecosystems with increased canopy cover generally have negative (i.e. cooling) biophysical climate feedbacks under current atmospheric CO₂ levels^{6–8}, further strengthening the capacity of terrestrial ecosystems as natural solutions to curb climate change. Large-scale afforestation is, therefore, offered as a promising and cost-effective climate mitigation solution^{9–11}. However, knowledge gaps exist in whether the strength and even if the sign of the biophysical climate feedbacks will persist from current to future atmospheric CO₂ concentrations. One such knowledge gap is the quantification of how CO₂-driven physiological changes will influence near-surface air temperature, and how these compare against broader mitigation gains by enhanced carbon sequestration that slows the rise in global mean temperatures.

Multiple vegetation characteristics drive synergistic changes of vegetation biophysics, mainly through changes in leaf area index (LAI) and stomatal conductance. Different levels of such changes may force different biophysical feedbacks on climate as CO₂ rises¹¹. Indeed, increasing atmospheric CO₂ induces simultaneously an enhancement of photosynthesis which often increases LAI, and a reduction in stomatal conductance^{12–14}. Recent analyses that focus on these physiological feedbacks (PHY) imply that they may exacerbate future heat extremes^{15,16} and amplify regional and global warming^{17,18}. However, the contributing processes of PHY feedbacks that affect local warming changes remain highly uncertain and are rarely considered in the assessments of the mitigation capacity of the terrestrial ecosystem. Evaluation of any extra PHY-induced warming is required, as its magnitude will influence emissions compatible with given overarching global temperature goals¹⁹.

Thus, our primary objective is to evaluate the overall mitigation capability of terrestrial ecosystems by comparing the PHY-

induced warming against the BGC-driven temperature cooling caused by terrestrial carbon accumulation. To do so, we investigate the vegetation feedbacks of PHY, at different atmospheric CO₂ levels and across the global vegetated land, on near-surface air temperature change. We use simulations from six Earth System Models (ESMs; see “Methods”) with a cumulative 1% per year increase in atmospheric CO₂ concentration ranging from 284 to 1132 ppm over 140 years²⁰. We find that PHY consistently amplifies global warming as CO₂ rises, partially offsetting cooling through CO₂-driven carbon storage increase. We attribute the PHY-induced temperature increase primarily to stomatal closure-induced evapotranspiration reductions. We find more PHY-based warming at locations with higher LAI (e.g. tropical forests) and less warming with lower LAI (e.g. Australia). We highlight that vegetation physiological response to increasing atmospheric CO₂ amplifies warming, which requires consideration with the cooling effect vegetation offers by “drawing down” atmospheric CO₂.

Results and discussion

Global vegetation physiological response to increasing atmospheric CO₂ and its reduction of mitigation potential. We calculate different effects of increasing CO₂ on mean annual near-surface air temperature change over global vegetated land. We compare the direct atmospheric radiative effect (RAD)-induced climate warming to the temperature reductions caused by the BGC effect. These two global temperature changes are, in turn, then compared against our main focus of aggregated local PHY-induced temperature contributions (PHY_{all}; Fig. 1). The main finding is that the spatial aggregation of PHY feedbacks on temperature over global vegetated land (green bars) offsets a substantial amount of the cooling effect through enhanced terrestrial carbon storage because of the BGC effects (blue bars). Terrestrial carbon storage continuously increases with rising atmospheric CO₂, and reaches a global total of 621 ± 260 Pg C under 4 × CO₂ (Supplementary Fig. 1). This increased land carbon storage is equivalent to 293 ± 122 ppm of CO₂ removal from the atmosphere and results in a temperature cooling of −1.24 ± 0.57 °C. The PHY_{all}-induced land temperature increase is

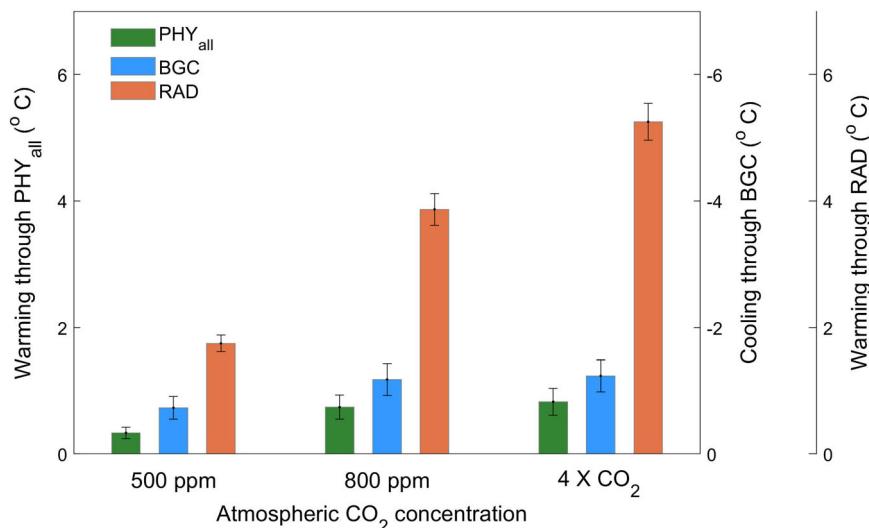


Fig. 1 Climate warming mitigation potential of terrestrial ecosystems. Global mean land temperature change due to total CO₂ physiological forcing (PHY_{all}), increased terrestrial carbon storage (BGC) and CO₂ radiative forcing (RAD). Note axes as coloured, and that the vertical blue axis is temperature cooling through BGC. It is straightforward to compare PHY_{all}, RAD- and BGC-induced temperature change when the same range and directions of bars are used. Three atmospheric CO₂ horizons are selected here, for CO₂ concentrations of 500 ppm, 800 ppm and 1032 ppm (4 × CO₂). Each bar represents the global area-weighted average from the ensemble of five ESMs. The error bars indicate the standard error of these five models. Note, the bcc-csm1-1 model did not provide diagnostics of carbon storage data and so is not included in calculating the temperature change by carbon storage change.

0.83 ± 0.47 °C, from the ensemble of five ESMs we use (here we excluded bcc-csm1-1; see “Methods”), corresponding to a large offset of the cooling effect by terrestrial ecosystems through BGC. However, our estimated temperature cooling induced by the BGC effect is a transient response. This cooling effect will be larger for subsequently stabilised CO₂ concentrations, since terrestrial ecosystems continue to fix carbon until reaching equilibrium. We note that BGC-induced cooling may be overestimated in the absence of land-cover change effect in the simulations, as the latter may reduce terrestrial carbon stores (Supplementary Fig. 2). However, inter-model differences, such as different parameterisation or different biogeochemistry module²⁰, may prevent a definitive answer as to how land-cover change influence global temperature change through BGC (Supplementary Fig. 2–5). We also note that we focus our analysis on CMIP5 data mainly due to the fact that the parameters in Eqs. (1) and (2)^{21,22} (see “Methods”) for calculating BGC-induced cooling are only currently available for CMIP5 ESMs.

The RAD response to rising CO₂ projects a global warming of 5.25 ± 0.65 °C, again under $4 \times$ CO₂, corresponding to roughly four times the magnitude of BGC-induced cooling. Hence, PHY_{all}-induced temperature increase adds about $16 \pm 8\%$ to the RAD-induced warming globally. The relative magnitude of warming/cooling effects is similar for the lower CO₂ levels of 500 ppm and 800 ppm (Fig. 1), illustrating the importance of accounting for PHY_{all}-induced warming and how it affects the ability of terrestrial vegetation to mitigate global warming, irrespective of CO₂ concentration. Our identified PHY_{all} feedbacks are a combination of different altered land properties. The balance of changed land components will depend on location, and so spatial variations in the overall warming effect may suggest a reappraisal of some climate change adaptation measures. Hence to aid such assessments, we now consider in detail the global contributions of individual drivers of the PHY-based local warming, and then any geographical variations.

In Fig. 2a, we show changes in global vegetated land air temperature associated with PHY_{all} with increasing atmospheric CO₂ from our ensemble of six ESMs (see “Methods”). PHY_{dir} (see “Methods”; Supplementary Table 1) is based on the direct CO₂ effect on vegetation physiology. PHY_{all} represents all the vegetation physiology-related feedbacks, and captures any additional interactions between RAD and PHY_{dir}, due to all effects not being a simple linear addition of RAD and PHY responses. The difference, PHY_{all} minus PHY_{dir}, is termed PHY_{int}. Although inter-model difference exists, warming levels are projected to increase, by all the ESMs, as CO₂ concentration rises, and for both PHY_{dir} and PHY_{all} (Fig. 2a). The interactive effects result in PHY_{all}-induced temperature change being higher than PHY_{dir} throughout the period. For the smaller increases in atmospheric CO₂ of up to ~450 ppm, interactive effects dominate with PHY_{dir} being almost zero up to that concentration. However, above the CO₂ concentration of 450 ppm, PHY_{dir} increases global warming reaching 0.17 ± 0.06 °C for CO₂ of 500 ppm, and climbing to 0.62 ± 0.48 °C under quadrupled atmospheric CO₂ (Fig. 2a). At that $4 \times$ CO₂ level, interaction term PHY_{int} increases warming by approximately one-fifth of that induced by PHY_{dir}. Hence, the overall physiological feedbacks described by PHY_{all} produce a global temperature increase of 0.74 ± 0.47 °C under $4 \times$ CO₂ (again from multi-model mean of six ESMs; see “Methods”).

To better understand the factors influencing CO₂ physiological drivers of temperature change, we decompose the global PHY_{all} into individual biophysical components⁶ (see “Methods”). These five aspects are albedo, aerodynamic resistance (r_a), evapotranspiration (ET), downwelling shortwave radiation (SW) and near-surface air emissivity (ϵ_a). These five-component changes result in climate forcings with different signs and magnitudes (Fig. 2b),

and thus perturb the surface energy balance, where positive values correspond to an increase in temperature. Specifically, ET, SW, and albedo generates positive climate forcings that increase local temperature, while r_a and ϵ_a produce negative effects and thus offset local temperature increase. The relative role of each biophysical component in influencing PHY_{all}-induced temperature change remains largely invariant in the transition from low to high CO₂ concentrations. In addition, the changes in these five quantities affecting PHY_{dir} show similar variations with that of PHY_{all} as atmospheric CO₂ rises (Supplementary Fig. 6). Those results are generally valid for CMIP6 results but with a lower magnitude of change (Supplementary Fig. 7).

The vegetation physiological response to rising CO₂ causes changes in LAI and stomata closure, which adjust in parallel with more detailed attributes of the land surface. The ESM simulations of changes in LAI and transpiration compare moderately well with available field measurements^{23–32} (Supplementary Fig. 8). Here we focus on their effects on the near-surface thermal changes, expressed as climate forcings on near-surface energy fluxes (Fig. 2b). The LAI increase due to elevated CO₂ (Supplementary Fig. 9a) leads to decreases in albedo^{11,33} (Supplementary Fig. 10a; Supplementary Table 2) and r_a ⁷ (Supplementary Fig. 10c). These changes are continuous with rising atmospheric CO₂ and result in positive and negative effects on global land air temperature change, respectively (Fig. 2b). Specifically, the albedo reduction increases solar radiation absorption by the land surface^{11,33}, and imposes a positive forcing of 0.30 ± 0.14 W m⁻² for 500 ppm, and of 0.51 ± 0.45 W m⁻² for a quadrupling of CO₂ (Fig. 2b). The decreased r_a favours the turbulent transport of heat from land to atmosphere⁷, and leads to a persistent surface cooling with increasing atmospheric CO₂^{34,35}, which is -1.66 ± 0.44 W m⁻² for 500 ppm and -3.15 ± 2.05 W m⁻² for $4 \times$ CO₂. In contrast, ET decreases considerably (Supplementary Fig. 10e; Supplementary Table 2) due to decreased stomatal conductance responding to increasing atmospheric CO₂. These reductions in ET reduce evaporative cooling^{15,17}, and therefore result in a strong positive climate forcing on global warming (Fig. 2b), which increases with rising atmospheric CO₂ and reaches 0.88 ± 0.25 W m⁻² for atmospheric CO₂ of 500 ppm and 2.88 ± 1.49 W m⁻² with quadrupled atmospheric CO₂ concentration (Fig. 2b).

Moreover, ET reduction decreases the inflow of evaporative water to the atmosphere, reducing cloud fraction and water vapour content, thereby feeding back to impose indirect effects that influence temperature change. We quantify these indirect effects through their effects on the components of SW and ϵ_a (Fig. 2b). The lower ET values reduce cloud fraction (Supplementary Table 2; Supplementary Fig. 9c) thereby increasing the amount of SW to the land surface^{6,35,36} (Supplementary Fig. 10g), and producing a moderate positive forcing of 0.67 ± 0.16 W m⁻² for 500 ppm and 1.76 ± 1.26 W m⁻² under $4 \times$ CO₂ (Fig. 2b). However, the reduced cloud fraction and water vapour content decreases ϵ_a (Supplementary Fig. 10i), which weakens the absorption of longwave radiation³⁷ (Supplementary Fig. 9e). The ϵ_a changes result in a small negative forcing (-0.28 ± 0.11 W m⁻² for 500 ppm and -0.57 ± 0.43 W m⁻² for $4 \times$ CO₂), and thereby lowering global temperatures. Of particular note is that the direct changes in ET produce the strongest positive forcing for warming (Fig. 2b). Hence, ET changes have a dominant role in influencing the magnitude and sign of PHY_{all} feedbacks on global temperature change. The changes in these five factors for PHY_{dir} are very close in relative terms to those of PHY_{all} (Supplementary Fig. 10), driving climate forcings in a similar magnitude and sign to influence PHY_{dir}-induced global temperature change (Supplementary Fig. 6).

Overall, as CO₂ rises, these five biophysical factors cause vegetation to amplify warming locally, and when aggregated

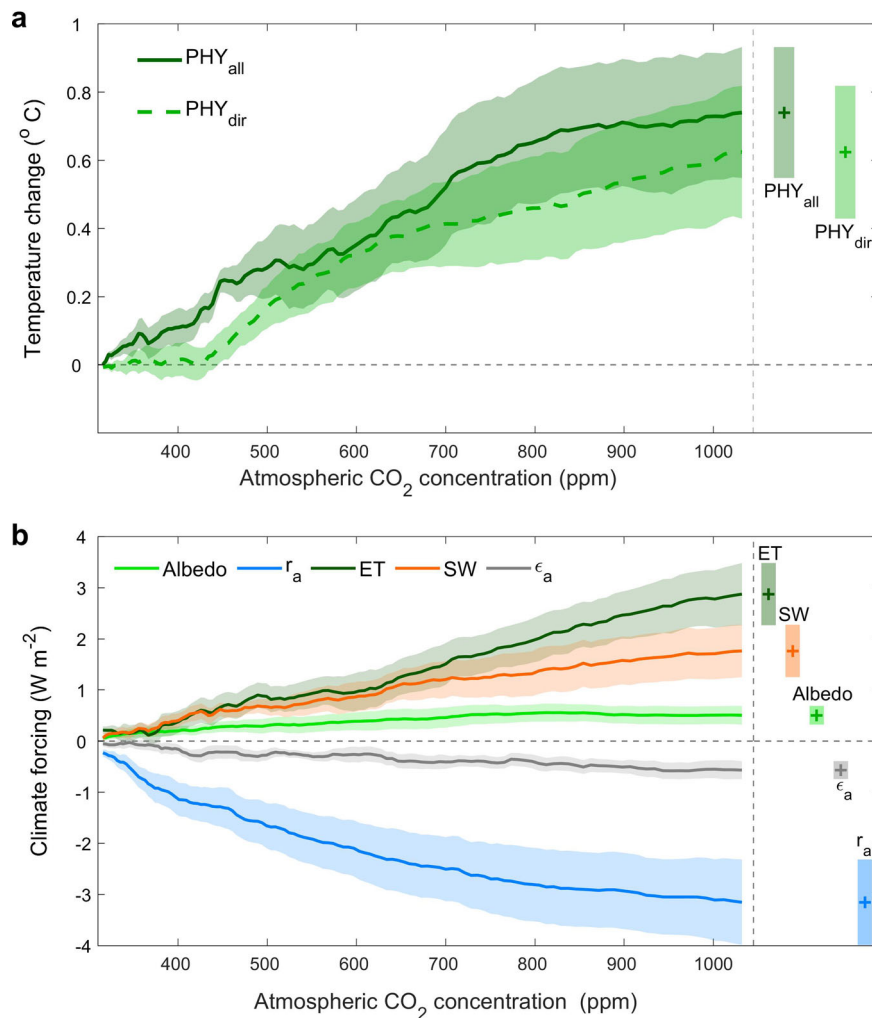


Fig. 2 Change in global mean annual land air temperature and individual climate forcing induced by vegetation physiological response to increasing atmospheric CO₂. **a** Global annual area-weighted temperature change of vegetated land induced by total CO₂ physiological forcing (PHY_{all}) and the direct CO₂ physiological forcing (PHY_{dir}) in response to increasing atmospheric CO₂ concentration. Shaded areas are the standard errors of the six Earth System Models (ESMs) used, and the thick curves are their multi-model means. For each atmospheric CO₂ concentration in panel (a), values are based on smoothing using a twenty-year running window (to match with the decomposition results in panel (b)). The final temperature change induced by PHY_{all} and PHY_{dir} effects under 4 × CO₂ are further marked on the righthand side, with the “+” markers indicating multi-model means. **b** PHY_{all}-induced climate forcing associated with changes in albedo, aerodynamic resistance (r_a), evapotranspiration (ET), downwelling shortwave radiation (SW) and near-surface air emissivity (ϵ_a). Again, the shaded areas are the standard errors of the models, and the mean is the thick continuous lines. The changes in these variables are calculated using a moving average with a 20-year window. The resulting values under 4 × CO₂ are plotted on the righthand side.

spatially act to raise planetary global warming. This additional warming effect is primarily driven by changes in ET, with smaller warming contributions from changes in SW and albedo, but also compensated with cooling effects from r_a and ϵ_a changes. The substantial role of ET on biophysical climate feedbacks is consistent with a previous study⁶, which investigates the biophysical feedbacks because of vegetation greening. That study proposed that CO₂-driven greening will enhance ET and thereby producing a net cooling effect. We build on that analysis by here additionally including the CO₂-induced partial stomatal closure^{17,18}. We find this inclusion overtakes the LAI influence on ET changes, resulting in large reductions in ET that will instead contribute to net warming as CO₂ rises. Large inter-model differences in simulating r_a dynamics (Supplementary Fig. 10c, d) mostly explains the substantial spread of r_a -induced climate forcing (Fig. 2b). The different extents of LAI increase (Supplementary Fig. 9a, b) also contribute to such differences in simulated r_a changes and effects on temperature change. Our noted large cooling through r_a changes is also indicated in a

recent study⁷, suggesting the importance of r_a in affecting vegetation biophysical climate feedbacks, and the importance of constraining this factor in climate models.

Spatial patterns and attributions of vegetation physiologically induced warming. We present in Fig. 3 the area-weighted regional contributions to global temperature change of the physiological responses and BGC under 4 × CO₂. PHY_{all}-based warming and BGC-induced cooling both show larger values in East and Central North America (ENA and CNA), North and Central Europe (NEU and CEU), Amazon (AMZ) and North Asia (NAS). Whereas, the smallest changes are in the Sahel region (SAH) (Fig. 3a). PHY_{all}-induced warming reduces large proportions of the temperature cooling through BGC in the northern mid-to-high latitudes (Fig. 3b). Furthermore, this cooling effect is fully offset by warming through vegetation physiological response in Alaska (ALA), Canada/Greenland/Iceland (CGI), NAS, NEU, SAH, Tibetan Plateau (TIB), Central (CAS) and West Asia

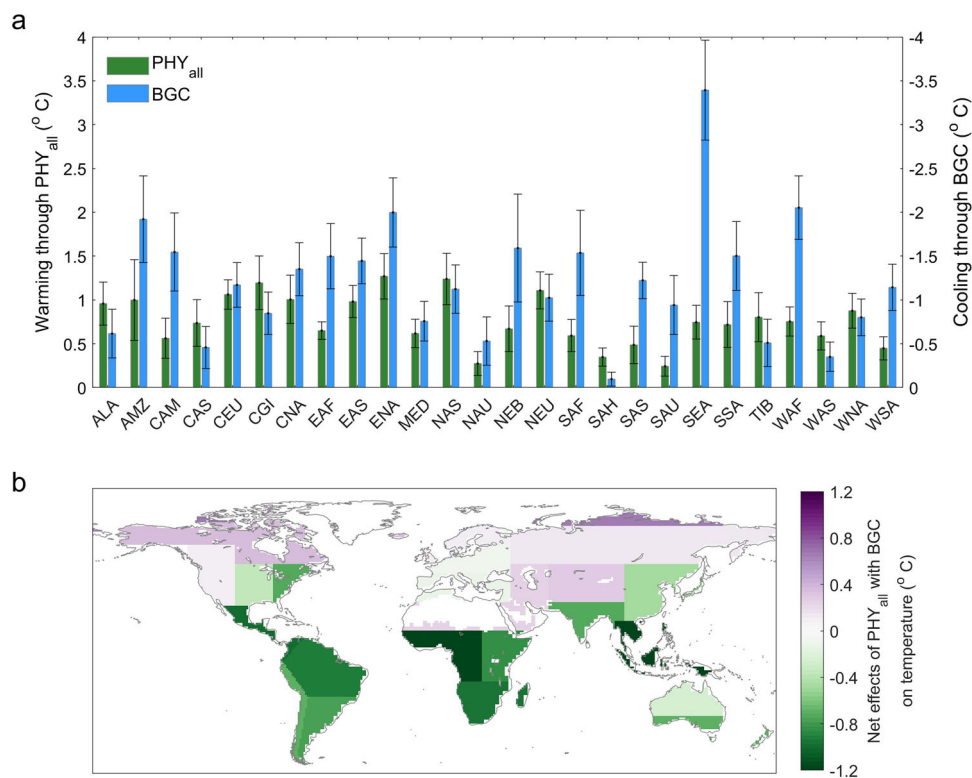


Fig. 3 Regional contributions to temperature change by PHY and BGC under $4 \times \text{CO}_2$. **a** Contribution of regional vegetation physiological responses (PHY_{all} ; green bars) and increased carbon storage (BGC; blue bars) to the overall global temperature change for each of the IPCC AR5 SREX regions. Bars represent area-weighted multi-model means, and the error bars indicate the standard errors of the models for each region. **b** Spatial distribution of the net effects of warming induced by PHY_{all} and cooling through BGC.

(WAS), and West North America (WNA), resulting in slight warming in these regions. Presented as a map of the net effects of BGC and PHY_{all} (Fig. 3b), we further illustrate this overall cooling effect from PHY and BGC for the tropical regions and South Hemisphere. Additionally, the balance of PHY and BGC to influence regional temperature change under relatively low atmospheric CO_2 level of 500 ppm (Supplementary Fig. 11) is very close to that for $4 \times \text{CO}_2$, suggesting consistency of vegetation biophysical and biogeochemical effects on climate irrespective of CO_2 levels. In summary, the PHY_{all} feedbacks offset the cooling benefits from ecosystem “draw-down” of CO_2 to a large extent, in line with the global average values presented in Fig. 1. Northern mid-to-high latitudes may contribute less than expected to slow global warming (Fig. 3). However, as also noted for the global change values, the estimated temperature cooling by BGC is a transient effect that would keep increasing as the ecosystems approach their equilibrium. However, BGC-induced cooling may be overestimated without consideration of the effect of land-cover change (Supplementary Fig. 2), which is often associated with the deliberate removal of terrestrial carbon.

The regional pattern in Fig. 3b provides a motivation to investigate further the five climate forcings-driven PHY_{all} contributions (Fig. 2a) to near-surface temperature change triggered by rising CO_2 . Here, we first examine the much finer spatial patterns and component contributions of PHY_{all} , PHY_{dir} and PHY_{int} on warming for $4 \times \text{CO}_2$. Focussing on PHY_{dir} and typically for $4 \times \text{CO}_2$, there is a larger local warming in the tropical forests (Fig. 4a), where vegetation shows higher potential to stabilise carbon than other ecosystems¹⁰ (Fig. 3). Within these tropical regions, the PHY_{dir} -forced temperature increase is the highest in the Amazon forests (Fig. 4a), reaching approximately

30% of that induced by RAD (Supplementary Fig. 12b). Strong warming by PHY_{dir} is also found in the northern mid-to-high latitudes ($>40^\circ\text{N}$). In contrast, smaller temperature increases due to PHY_{dir} are seen in arid and semi-arid regions, such as Australia and Sahel (Fig. 4a). The spatial variations of PHY_{all} -forced temperature change (Supplementary Fig. 13a) have strong similarities to those of PHY_{dir} (Fig. 4a). These similarities again suggest a relatively small role of interactions on temperature change (Supplementary Fig. 13b) under quadrupled CO_2 . Additionally, the agreements across the six ESMs are reasonably high, with all the models agreeing that PHY_{all} , PHY_{dir} and PHY_{int} result in local warming for $4 \times \text{CO}_2$ across most of the global vegetated land (Supplementary Fig. 14).

We next analyse spatially the decomposition of PHY_{all} - and PHY_{dir} -induced temperature change into the five biophysical factors shown in Fig. 2b, and with findings shown in Fig. 4b–f. In response to quadrupled CO_2 , LAI shows increases over most global vegetated land (Supplementary Fig. 15b), leading to a positive climate forcing (and thus warming) through reducing albedo (Fig. 4b), and especially in the south Sahel and Tibetan Plateau. Moreover, a large albedo decrease occurs in the northern mid-to-high latitudes, such as for most of Siberia. This albedo decrease may be due to LAI increase combined with reduced snow cover promoted by PHY-driven warming¹⁷. The LAI increase also contributes to a strong negative forcing through r_a decrease⁷. This r_a decrease enhances the energy exchange between land and atmosphere, lowering the local warming effect in response to $4 \times \text{CO}_2$, particularly in Australia, Sahel, South Africa and South Asia (Fig. 4c). In comparison, the projected forcing from ET reductions (Supplementary Fig. 15d) causes strongly positive warming, and especially in the tropical and boreal forests (Fig. 4d). The larger ET reductions in the tropical and boreal

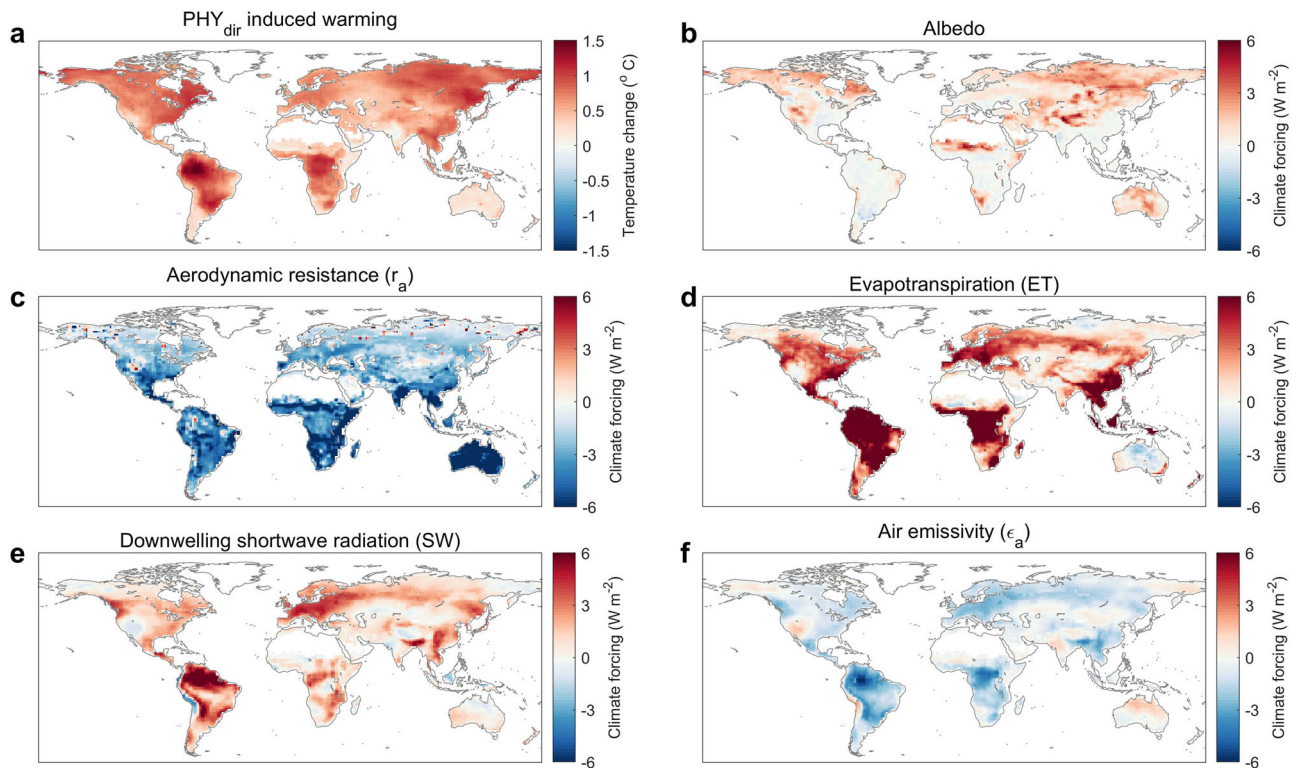


Fig. 4 Global patterns of local temperature change and climate forcings through vegetation physiological response to $4 \times \text{CO}_2$. Spatial distribution of annual mean temperature change from multi-model ensemble induced by (a) direct CO_2 physiological forcing (PHY_{dir}) in response to a $4 \times \text{CO}_2$ rise since pre-industrial level. The spatial patterns of the individual climate forcing contributing to PHY_{dir} of panel (a) are as follows. In (b) albedo (α), (c) Aerodynamic resistance (r_a), (d) Evapotranspiration (ET), (e) Downwelling shortwave radiation (SW) and (f) near-surface air emissivity (ϵ_a). In all panels, estimates use the mean of the final 20 years of the simulations (atmospheric CO_2 at ~ 1032 ppm).

forests also lead to stronger cloud fraction decreases (Supplementary Fig. 15f). These feedbacks induce a positive climate forcing for additional warming by increasing SW reaching the land surface (Fig. 4e). Simultaneously, the decreased cloud cover and water vapour by the ET reductions generate a cooling effect (Fig. 4f) through decreasing net longwave radiation absorption in most locations. The PHY_{dir} -induced warming and the associated climate forcings at an atmospheric CO_2 concentration of 500 ppm (Supplementary Fig. 16) show similar spatial distributions, but smaller magnitude, compared with that adjustment for $4 \times \text{CO}_2$ increase (Fig. 4). This result manifests that PHY continues to amplify global warming through the combined climate forcings from our identified five biophysical factors, irrespective of CO_2 concentration.

Substantial differences exist between PHY_{all} - and PHY_{dir} -induced temperature changes in northwestern Eurasia, implying pronounced PHY_{int} -based feedbacks there under $4 \times \text{CO}_2$ (Supplementary Fig. 13b). A relatively large change in SW, inducing a warming effect (Supplementary Fig. 13j), mainly contributes to the large PHY_{int} -coupled changes in this region. Elsewhere, for the Amazon forests, the cooling effect in PHY_{int} through changes in ET (Supplementary Fig. 13h) and SW (Supplementary Fig. 13j), cancels out the warming due to changes in r_a (Supplementary Fig. 13f) and ϵ_a (Supplementary Fig. 13l). This cancellation causes negligible PHY_{int} feedback on temperature there (Supplementary Fig. 13b). In summary, local warming due to biophysical feedback of increasing CO_2 is regulated primarily by the positive forcing from ET reductions (with smaller positive forcings from albedo and SW changes), which is partly compensated by reductions in r_a (and a small contribution from ϵ_a).

Strong physiologically induced warming in dense ecosystems.

We further investigate the finding presented in Fig. 4 that PHY_{dir} -forced temperature increase is higher in the tropical forests, while lower in the arid and semi-arid ecosystems. This finding suggests that there may be a relationship between the forced temperature change and background baseline LAI, which we confirm in Fig. 5a (for both PHY_{all} and PHY_{dir}). We find widespread warming amplification with increasing LAI for lower background LAI levels. Such rates of increase in temperature per unit of LAI show evidence of flattening at higher LAI values³⁸. That is, the CO_2 -fertilised LAI increase saturates in ecosystems with dense canopy cover such as tropical forests (Supplementary Fig. 17a). However, the stomatal closure-induced ET decrease varies almost linearly with baseline LAI, although the reduction breaks down when the baseline LAI approaches six (Supplementary Fig. 17b). Hence, we conclude that ET reductions caused by stomatal closure are the primary cause of PHY-induced temperature rises, although changes in r_a because of LAI increases remain an important factor (Fig. 4; Supplementary Fig. 13). Taking all the components together, PHY_{dir} -triggered temperature change increases almost linearly with baseline LAI gradients under $4 \times \text{CO}_2$ (Fig. 5a). Of particular interest is that when expressing PHY_{dir} -induced temperature increase as a fraction of warming induced by RAD, it also increases with the baseline LAI value (Fig. 5b). Hence, Fig. 5 provides strong evidence that background vegetation functional structure (LAI) influences the feedback of CO_2 physiological forcing on warming in response to $4 \times \text{CO}_2$. In terms of change, as the trend of global LAI increase slows down as atmospheric CO_2 concentration increases to very high levels (Supplementary Fig. 9a, b), this suggests that the magnitude of the cooling effect (via r_a) will decrease relative to the ET-based warming.

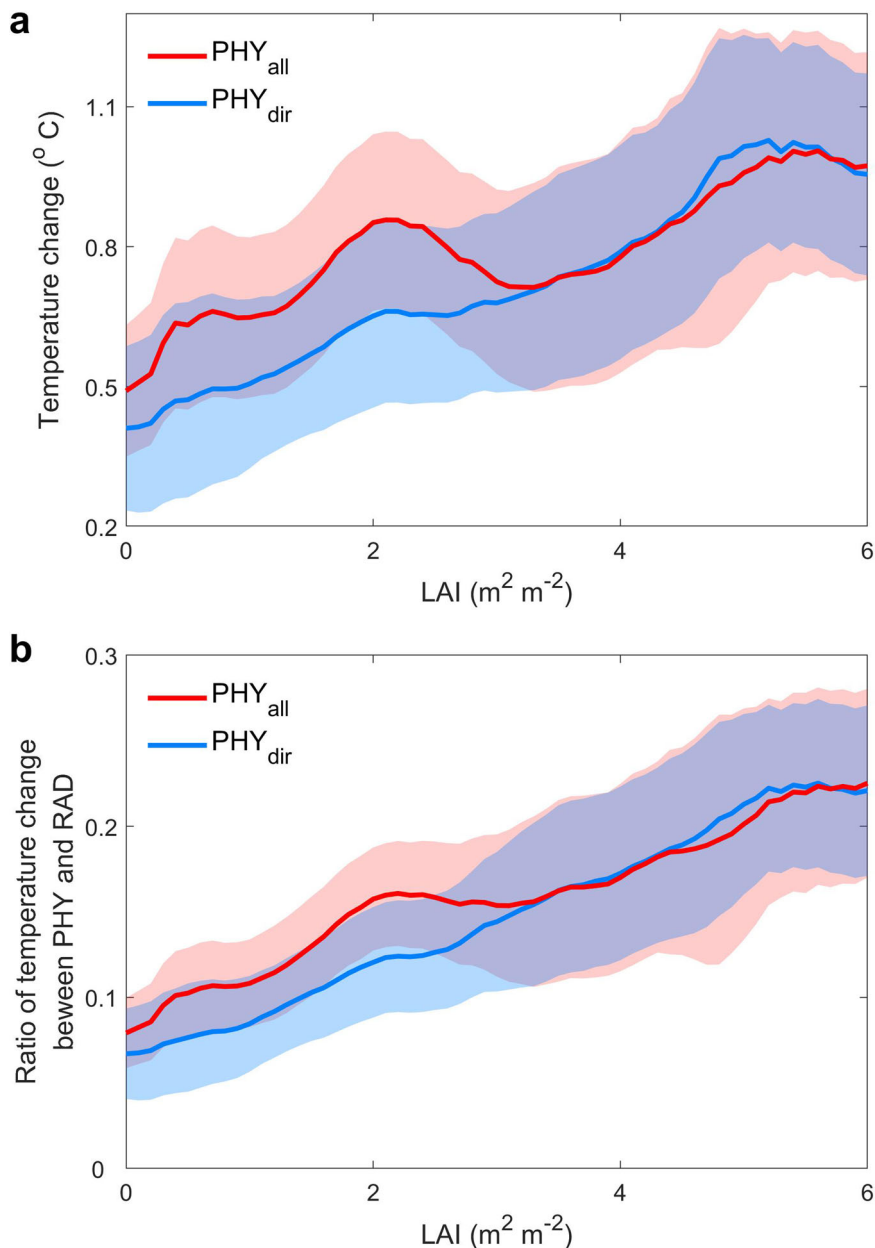


Fig. 5 Effects of vegetation structure on CO_2 physiological forcing in response to $4 \times \text{CO}_2$. **a** Variations of local temperature change induced by total (PHY_{all}) and direct (PHY_{dir}) CO_2 physiological forcing, for quadrupled CO_2 and presented as a function of baseline pre-industrial leaf area index (LAI). **b** Variations of the ratio of PHY_{all} - and PHY_{dir} -induced temperature change relative to that of RAD warming, again for $4 \times \text{CO}_2$ and as a function of baseline LAI. In both panels, the temperature changes along LAI gradients are smoothed using a five-bin running window for the 0.1 increments in LAI bin size. The shaded areas indicate the standard error among different models.

Implications and conclusions. Terrestrial ecosystems respond to increasing atmospheric CO_2 not only through accumulating carbon (the “BGC” effect) but also through their physiological response (the “PHY” feedback), which can have opposing effects on local surface temperature. As such, to fully understand the net climate benefits of terrestrial ecosystems, comprehensive assessments need to account for both PHY and BGC effects^{39,40}. We find that the warming through PHY feedback largely reduces the capacity of vegetation to slow global warming through BGC. In particular, vegetation transiently operates to amplify local warming in the northern mid-to-high latitudes, as PHY-induced warming is larger than BGC-induced cooling (Fig. 3). Tropical forests have net cooling effects, and forests and ecosystem restoration efforts there would have

much higher net cooling benefit for mitigation than if they are placed in the northern mid-to-high latitudes. At the global scale, this PHY-induced warming can offset by up to 67% of the cooling gains from the transient BGC effect (Fig. 1). This is likely an upper-bound value, because the steady-state BGC effect is larger than the transient one. Thus, afforestation can still result in a net cooling effect, especially in the tropics, although the cooling achieved may be less than first expected. Of particular interest is that the PHY-based warming is generally stronger for high baseline LAI values (Fig. 5). This result further suggests the PHY produces extra warming through afforestation due to higher LAI for forests than non-forests. However, this does not contradict the finding for the tropics (where LAI is high) as possibly the most beneficial

regions for afforestation, due to the compensating much larger BGC potential to lower temperature for such locations.

Our analysis highlights the importance of including PHY feedbacks in any assessments of future levels of global warming. Such understanding may be especially important for the northern mid-to-high latitudes. We point out that only one-third of ESMs we use incorporate dynamic global vegetation schemes (DGVMs). Since land-cover change acts to influence PHY and BGC effects (Supplementary Fig. 2–5), future simulations with dynamic vegetation may allow refining these results. However, we note that inter-model structural differences (e.g. different ratio of transpiration to ET^{15,41}) contribute to large uncertainties in these results. In particular, we note the potential implications of our results for climate mitigation policies with substantial reforestation as a mechanism to slow global warming through emissions offsetting. Reforestation may cause a near-surface cooling through the BGC effect. However, the PHY-based warming effect is stronger for higher LAI values as atmospheric CO₂ rises (Fig. 5a). This must be accounted for in any major global reforestation plans with consideration of particular location of reforestation measures⁴². In general, the effects of anthropogenic land use and land cover change on vegetation biophysical and biogeochemical processes are important and complex with substantial spatial heterogeneity^{42–47}. Given the lack of exploitable factorial simulations designed to separate land use and land-cover change effects, these are ignored in the idealised simulations, and may introduce a bias in our results. We note, however, that these idealised “4 × CO₂” simulations broadly capture the sign and spatial distributions of land-atmosphere coupling effects on temperature change through comparisons to the ESM results under the RCP8.5 scenario (Supplementary Fig. 18) which include anthropogenic land use and land-cover change. We suggest that future climate projections should much more routinely account for the effect of anthropogenic land use and land-cover change together with PHY and BGC effects^{42,47}, and so that this can be considered in reforestation climate mitigation strategies.

An additional caveat of our research is that the PHY and RAD factorial ESM simulations that inform our analysis, are at present only available for the illustrative but potentially unrealistic exponential increase in atmospheric CO₂ (1% per year). For this scenario, the systems can exhibit a unrealistic linear behaviour⁴⁸. PHY and RAD simulations under other scenarios, such as abrupt 4 × CO₂ or even historical forcing followed by a potential future scenario, would greatly help to improve projections of PHY feedbacks. We suggest this should be made a high priority of climate modelling exercises, especially if additionally including land use and land-cover change representation. We recognise that the newer CMIP6 ESMs contain improved representation of many processes (e.g. atmospheric aerosols, clouds, and land processes)⁴⁹. We anticipate our findings to remain broadly valid with the CMIP6 models, although the magnitude of PHY-induced warming is lower for CMIP6 than CMIP5 ESMs¹⁸, especially in the northern high latitudes. We hope our analysis provides an incentive to others to undertake such analysis as all the calculations (BGC, PHY, and RAD) become available for that newer CMIP6 ensemble. In summary, our results illustrate that vegetation physiological response to increasing atmospheric CO₂ has a substantial local warming effect, which requires consideration alongside the cooling effect vegetation offers by “drawing down” atmospheric carbon dioxide.

Methods

CMIP5 outputs. The results from six Earth System Models (ESMs) that participated in the Coupled Model Intercomparison Project Phase 5 (CMIP5) were obtained from the CMIP5 archive (<https://esgf-node.lnl.gov/search/cmip5/>). We

used the ESMs of bcc-csm1-1⁵⁰, CanESM2⁵¹, CESM1-BGC⁵², HadGEM2-ES⁵³, IPSL-CM5A-LR⁵⁴, and MPI-ESM-LR⁵⁵. For each model, we adopted the simulations of 1% per year cumulative increase in atmospheric CO₂ concentration, which corresponds to a rise from 284 to 1132 ppm over 140 years. Anthropogenic land-use and land-cover changes are not included in these simulations. HadGEM2-ES and MPI-ESM-LR incorporate full dynamic global vegetation models, allowing natural vegetation coverage and competition changes with CO₂ levels²⁰. The remaining four ESMs do not include DGVMs, and therefore the nature vegetation distributions remain fixed over time, although they do project LAI changes. Any effects related to actual land-use change on temperature are not considered in this study. We selected this scenario, and these models, as projections are available with these ESMs that not only account for both radiative and physiological together (“1pctCO₂”), but critically there are also factorial simulations of radiative only (“esmFdbk1”) and physiological only (“esmFixClim1”) effects^{20,56}. The radiative only simulations include just the radiative effects of CO₂, which means only the atmospheric system experiences the 1% per year cumulative increase in atmospheric CO₂ concentration. In contrast, only the land surface responds to increasing atmospheric CO₂ in physiological only simulations²⁰. The monthly outputs we used are from these three scenarios include near-surface air temperature at 2 m, evapotranspiration (ET), transpiration, LAI, upwelling and downwelling shortwave radiation, upwelling and downwelling longwave radiation, cloud fraction, latent heat, sensible heat, vegetation, and soil carbon storage. These variables were averaged temporally to annual scale. We also re-gridded, spatially, to a common 1° × 1° grid, before further averaging inter-ESMs to obtain a multi-model ensemble.

We calculated the difference between the 1pctCO₂ and esmFdbk1 simulations to evaluate the total PHY feedback (PHY_{all}), as this allows the inclusion of any nonlinear interactions between CO₂ physiological and radiative forcings^{15,17}. The effects of RAD, however, were calculated as simply the difference between each of the 140 years in the esmFdbk1 experiment and its average over the first 20 years. We use esmFdbk1 simulations, rather than 1pctCO₂ minus esmFixClim1, to directly calculate the RAD effects, to exclude any interactions between PHY and RAD, i.e. some warming-induced vegetation feedbacks. The estimated temperature change from five model ensemble was highly comparable with that from ensemble of six ESMs (see below for why the bcc-csm1-1 was not included in all the analyses). The direct PHY feedback (PHY_{dir}) was calculated as the difference between each year over the whole study period in the esmFixClim1 and its average over the first 20 years. The interaction (PHY_{int}) of CO₂ physiological and radiative forcing was estimated as the difference between the PHY_{all} and PHY_{dir} calculations. We smoothed all the PHY_{dir}- and PHY_{all}-induced variable changes using a twenty-year running window. In addition, we used the averaged data of the final 20 years (~ 1032 ppm atmospheric CO₂ concentration, nearing 4 × CO₂) when presenting the spatial patterns of PHY_{all}, PHY_{dir}, and PHY_{int}-related changes. The averaged LAI of the first 20 years, in the 1pctCO₂ scenario from the ensemble of the six selected models, was considered as the baseline LAI (as required for Fig. 5). We screened out non-vegetated land locations with LAI < 0.1. Moreover, when considering any dependence on background LAI, we binned PHY_{all}- and PHY_{dir}-induced temperature change at a step of 0.1 LAI ranging from 0.0 to 6.0. This range accounted for 98% of LAI global distributions. We binned PHY_{all}- and PHY_{dir}-induced temperature change in the pixels with LAI value larger than 6.0 into the bin of 6 to include all the available vegetated pixels in the analysis.

Potential of terrestrial ecosystem carbon storage for climate mitigation.

Estimates of carbon storage in vegetation (cVeg) and soil (cSoil) were obtained from the three scenarios of five ESMs (the bcc-csm1-1 model was not included since it does not have cVeg and cSoil outputs). The total carbon storage (cTot) of terrestrial ecosystem was calculated as the sum of cVeg and cSoil. As for other quantities, the annual cTot of each model was re-gridded to a common 1° × 1° grid for calculating a multi-model ensemble. The PHY_{all}-induced cTot changes were calculated similarly, and based on the difference between the 1pctCO₂ and esmFdbk1 scenarios.

To estimate the implication of increasing carbon storage changes due to the biogeochemical effect (BGC) on slowing the rate of warming (ΔT_a), as derived from the PHY simulations, we calculate this as a function of the time-evolving CO₂ increase and ESM-projected alteration to carbon storage change ΔcTot. We used the method from previous studies^{21,22}, with the derived equation of:

$$\Delta T_a = \int_{t=0}^{t'} \frac{a_s}{\tau_s} \exp\left(-\frac{t}{\tau_s}\right) + \frac{a_f}{\tau_f} \exp\left(-\frac{t}{\tau_f}\right) \text{RF}(t' - t) dt \quad (1)$$

$$\text{RF}(t) = \frac{F}{\log_4} \log\left(1 + \frac{\Delta c\text{Tot}(t)}{\text{CO}_2(t)}\right) \quad (2)$$

Quantities, a_s , a_f , τ_s , τ_f , λ (radiative feedback parameter) and F (radiative forcing) were parameters²². Note, the estimated temperature change is transient and has inertia, as illustrated by the time-delay function in the integral of Eq. (1). Hence ΔT_a would ultimately be larger for ecosystems approaching to an equilibrium. Three horizons of atmospheric CO₂ concentration were selected of 500 ppm, 800 ppm and 1032 ppm (latter 4 × CO₂), to account for ΔT_a under different atmospheric CO₂ concentrations. We converted the total carbon storage changes (Pg C) to equivalent atmospheric CO₂ concentration (ppm) using a

conversion ratio⁵⁷ of 2.123 Pg C ppm⁻¹. The regional contributions (Fig. 3) of increased carbon storage to global temperature change was then determined using the proportion of regional to global carbon storage change. The standard IPCC AR5 SREX regions (https://www.ipcc-data.org/guidelines/pages/ar5_regions.html) were used to provide the regional boundaries to such contributions.

Decomposition of CO₂ physiological forcing feedback. We decomposed the feedbacks of PHY_{all} and PHY_{dir} into changes in five factors⁶, which was based on perturbations to the surface energy balance. Here, the resulted temperature change (still referred to ΔT_a), was decomposed using the following equation:

$$\Delta T_a = \frac{1}{f} \left(-\text{SW}\Delta\alpha - \lambda\Delta\text{ET} + \Delta\text{SW}(1 - \alpha) + \varepsilon_s\sigma T_a^4\Delta\varepsilon_a + \frac{\rho C_d(T_s - T_a)}{r_a^2} \Delta r_a \right) + \lambda\Delta T_a \quad (3)$$

Here T_a represents air temperature, f is the conversion ratio of climate forcing to actual air temperature, SW is downwelling shortwave radiation (W m^{-2}), α is albedo, λ is the latent heat of vaporisation (J kg^{-1}), ET is evapotranspiration (mm d^{-1}), ε_s is land surface emissivity, σ is Stephan-Boltzmann constant ($5.67 \times 10^{-8} \text{ W m}^{-2} \text{ K}^{-4}$), ε_a is near-surface air emissivity, ρ is air density (1.21 kg m^{-3}), C_d is specific heat of air at constant pressure ($1.013 \text{ J kg}^{-1} \text{ K}^{-1}$), T_s is land surface temperature, r_a is aerodynamic resistance (s m^{-1}) and T_a^{cir} represents the influence of atmospheric circulation. Variable r_a is estimated by inversion of the equation of sensible heat (H):

$$H = \rho C_d \frac{T_s - T_a}{r_a} \quad (4)$$

In addition, ε_a was given by the net longwave radiation calculation:

$$L_{\text{in}} - L_{\text{out}} = \varepsilon_s\sigma(T_a^4\varepsilon_a - T_s^4) \quad (5)$$

where L_{in} was downwelling longwave radiation (W m^{-2}), and L_{out} was upwelling longwave radiation (W m^{-2}).

The five decomposed items, $-\text{SW}\Delta\alpha$, $-\lambda\Delta\text{ET}$, $\Delta\text{SW}(1 - \alpha)$, $\varepsilon_s\sigma T_a^4\Delta\varepsilon_a$, and $\frac{\rho C_d(T_s - T_a)}{r_a^2} \Delta r_a$, respectively represent the climate forcing induced by changes in albedo ($\Delta\alpha$), evapotranspiration (ΔET), downwelling shortwave radiation (ΔSW), air emissivity ($\Delta\varepsilon_a$) and aerodynamic resistance (Δr_a). Detailed derivation of Eqs. (3)–(5) are provided in the previous studies^{6,35}, and we follow directly the methodologies of those analyses. As with the total PHY feedback, we used a 20-year moving average spanning the full atmospheric CO₂ concentration ranges. The difference of the decomposition results between the PHY_{all} and PHY_{dir} simulations was calculated to identify the magnitude of the individual climate forcings contributing to the extra interaction-based warming, PHY_{int}. The decomposition results of the final 20 years were retained in spatial format (i.e. not averaged to global temperature changes) to understand the spatial patterns of PHY_{all} and PHY_{dir} feedback on temperature change in response to $4 \times \text{CO}_2$.

Data availability

The CMIP5 and CMIP6 model outputs are available in <https://esgf-node.llnl.gov/search/cmip5/> and <https://esgf-node.llnl.gov/search/cmip6/>, respectively.

Code availability

All the analyses and figures are made using MATLAB 2019b, and the codes are available from the corresponding author on reasonable request.

Received: 3 July 2021; Accepted: 29 June 2022;

Published online: 13 July 2022

References

- Burrell, A. L., Evans, J. P. & De Kauwe, M. G. Anthropogenic climate change has driven over 5 million km² of drylands towards desertification. *Nat. Commun.* **11**, 3853 (2020).
- Liu, Y. et al. Field-experiment constraints on the enhancement of the terrestrial carbon sink by CO₂ fertilization. *Nat. Geosci.* **12**, 809–814 (2019).
- Wenzel, S., Cox, P. M., Eyring, V. & Friedlingstein, P. Projected land photosynthesis constrained by changes in the seasonal cycle of atmospheric CO₂. *Nature* **538**, 499–501 (2016).
- Friedlingstein, P. et al. Global Carbon Budget 2019. *Earth Syst. Sci. Data* **11**, 1783–1838 (2019).
- Arneth, A. et al. Terrestrial biogeochemical feedbacks in the climate system. *Nat. Geosci.* **3**, 525–532 (2010).

- Zeng, Z. et al. Climate mitigation from vegetation biophysical feedbacks during the past three decades. *Nat. Clim. Chang.* **7**, 432–436 (2017).
- Chen, C. et al. Biophysical impacts of Earth greening largely controlled by aerodynamic resistance. *Sci. Adv.* **6**, eabb1981 (2020).
- Winckler, J., Lejeune, Q., Reick, C. H. & Pongratz, J. Nonlocal effects dominate the global mean surface temperature response to the biogeophysical effects of deforestation. *Geophys. Res. Lett.* **46**, 745–755 (2019).
- Canadell, J. G. & Raupach, M. R. Managing forests for climate change mitigation. *Science* **320**, 1456–1457 (2008).
- Griscom, B. W. et al. Natural climate solutions. *Proc. Natl Acad. Sci.* **114**, 11645–11650 (2017).
- Arora, V. K. & Montenegro, A. Small temperature benefits provided by realistic afforestation efforts. *Nat. Geosci.* **4**, 514–518 (2011).
- Field, C. B., Jackson, R. B. & Mooney, H. A. Stomatal responses to increased CO₂: implications from the plant to the global scale. *Plant. Cell Environ.* **18**, 1214–1225 (1995).
- Ainsworth, E. A. & Long, S. P. What have we learned from 15 years of free-air CO₂ enrichment (FACE)? A meta-analytic review of the responses of photosynthesis, canopy properties and plant production to rising CO₂. *New Phytol.* **165**, 351–372 (2005).
- Lammertsma, E. I. et al. Global CO₂ rise leads to reduced maximum stomatal conductance in Florida vegetation. *Proc. Natl Acad. Sci.* **108**, 4035 LP–4034040 (2011).
- Skinner, C. B., Poulsen, C. J. & Mankin, J. S. Amplification of heat extremes by plant CO₂ physiological forcing. *Nat. Commun.* **9**, 1094 (2018).
- Lemondant, L. & Gentine, P. Vegetation response to rising CO₂ impacts extreme temperatures. *Geophys. Res. Lett.* **46**, 1383–1392 (2019).
- Park, S.-W., Kim, J.-S. & Kug, J.-S. The intensification of Arctic warming as a result of CO₂ physiological forcing. *Nat. Commun.* **11**, 2098 (2020).
- Zarakas, C. M., Swann, A. L. S., Laguë, M. M., Armour, K. C. & Randerson, J. T. Plant physiology increases the magnitude and spread of the transient climate response to CO₂ in CMIP6 earth system models. *J. Clim.* **33**, 8561–8578 (2020).
- IPCC. *Global Warming of 1.5°C. An IPCC Special Report on the Impacts of Global Warming of 1.5°C Above Pre-industrial Levels and Related Global Greenhouse Gas Emission Pathways, in the Context of Strengthening the Global Response to the Threat of Climate Change, sustainable development, and efforts to eradicate poverty* (eds Masson-Delmotte, V. et al.) 616 pp (2018) (IPCC, Cambridge University Press, Cambridge, UK and New York, NY, USA, 2018).
- Arora, V. K. et al. Carbon-concentration and carbon-climate feedbacks in CMIP5 earth system models. *J. Clim.* **26**, 5289–5314 (2013).
- Geoffroy, O. et al. Transient climate response in a two-layer energy-balance model. Part II: Representation of the efficacy of deep-Ocean heat uptake and validation for CMIP5 AOGCMs. *J. Clim.* **26**, 1859–1876 (2013).
- Geoffroy, O. et al. Transient climate response in a two-layer energy-balance model. Part I: Analytical solution and parameter calibration using CMIP5 AOGCM experiments. *J. Clim.* **26**, 1841–1857 (2013).
- Uddling, J., Teclaw, R. M., Pregitzer, K. S. & Ellsworth, D. S. Leaf and canopy conductance in aspen and aspen-birch forests under free-air enrichment of carbon dioxide and ozone. *Tree Physiol.* **29**, 1367–1380 (2009).
- Lee, T. D., Tjoelker, M. G., Ellsworth, D. S. & Reich, P. B. Leaf gas exchange responses of 13 prairie grassland species to elevated CO₂ and increased nitrogen supply. *New Phytol.* **150**, 405–418 (2001).
- McCARTHY, H. R. et al. Temporal dynamics and spatial variability in the enhancement of canopy leaf area under elevated atmospheric CO₂. *Glob. Chang. Biol.* **13**, 2479–2497 (2007).
- Schäfer, K. V. R., Oren, R., Lai, C.-T. & Katul, G. G. Hydrologic balance in an intact temperate forest ecosystem under ambient and elevated atmospheric CO₂ concentration. *Glob. Chang. Biol.* **8**, 895–911 (2002).
- Duursma, R. A. et al. Canopy leaf area of a mature evergreen Eucalyptus woodland does not respond to elevated atmospheric [CO₂] but tracks water availability. *Glob. Chang. Biol.* **22**, 1666–1676 (2016).
- Liberloo, M. et al. Elevated CO₂ concentration, fertilization and their interaction: growth stimulation in a short-rotation poplar coppice (EUROFACE). *Tree Physiol.* **25**, 179–189 (2005).
- Newingham, B. A. et al. No cumulative effect of 10 years of elevated [CO₂] on perennial plant biomass components in the Mojave Desert. *Glob. Chang. Biol.* **19**, 2168–2181 (2013).
- Norby, R. J., Sholtis, J. D., Gunderson, C. A. & Jawdy, S. S. Leaf dynamics of a deciduous forest canopy: no response to elevated CO₂. *Oecologia* **136**, 574–584 (2003).
- Warren, J. M. et al. Ecohydrologic impact of reduced stomatal conductance in forests exposed to elevated CO₂. *Ecohydrology* **4**, 196–210 (2011).
- Bader, M. K.-F. et al. Central European hardwood trees in a high-CO₂ future: synthesis of an 8-year forest canopy CO₂ enrichment project. *J. Ecol.* **101**, 1509–1519 (2013).

33. Swann, A. L. S., Fung, I. Y. & Chiang, J. C. H. Mid-latitude afforestation shifts general circulation and tropical precipitation. *Proc. Natl Acad. Sci.* **109**, 712–716 (2012).
34. Forzieri, G. et al. Increased control of vegetation on global terrestrial energy fluxes. *Nat. Clim. Chang.* **10**, 356–362 (2020).
35. Li, Y., Piao, S., Chen, A., Ciais, P. & Li, L. Z. X. Local and teleconnected temperature effects of afforestation and vegetation greening in China. *Natl. Sci. Rev.* **7**, 897–912 (2019).
36. Cao, L., Bala, G., Caldeira, K., Nemani, R. & Ban-Weiss, G. Importance of carbon dioxide physiological forcing to future climate change. *Proc. Natl Acad. Sci.* **107**, 9513–9518 (2010).
37. Serreze, M. C. & Barry, R. G. Processes and impacts of Arctic amplification: a research synthesis. *Glob. Planet. Change* **77**, 85–96 (2011).
38. Mahowald, N. et al. Projections of leaf area index in earth system models. *Earth Syst. Dyn.* **7**, 211–229 (2016).
39. Jackson, R. B. et al. Protecting climate with forests. *Environ. Res. Lett.* **3**, 44006 (2008).
40. Windisch, M. G., Davin, E. L. & Seneviratne, S. I. Prioritizing forestation based on biogeochemical and local biogeophysical impacts. *Nat. Clim. Chang.* **11**, 867–871 (2021).
41. Dong, J., Lei, F. & Crow, W. T. Land transpiration-evaporation partitioning errors responsible for modeled summertime warm bias in the central United States. *Nat. Commun.* **13**, 336 (2022).
42. Bonan, G. B. Forests and climate change: forcings, feedbacks, and the climate benefits of forests. *Science* **320**, 1444 LP–1441449 (2008).
43. Chen, L. & Dirmeyer, P. A. Adapting observationally based metrics of biogeophysical feedbacks from land cover/land use change to climate modeling. *Environ. Res. Lett.* **11**, 34002 (2016).
44. Obermeier, W. A. et al. Modelled land use and land cover change emissions—a spatio-temporal comparison of different approaches. *Earth Syst. Dyn.* **12**, 635–670 (2021).
45. Gasser, T. & Ciais, P. A theoretical framework for the net land-to-atmosphere CO₂ flux and its implications in the definition of “emissions from land-use change”. *Earth Syst. Dyn.* **4**, 171–186 (2013).
46. Rigden, A. J. & Li, D. Attribution of surface temperature anomalies induced by land use and land cover changes. *Geophys. Res. Lett.* **44**, 6814–6822 (2017).
47. Feddema, J. J. et al. The importance of land-cover change in simulating future climates. *Science* **310**, 1674–1678 (2005).
48. Raupach, M. R. The exponential eigenmodes of the carbon-climate system, and their implications for ratios of responses to forcings. *Earth Syst. Dyn.* **4**, 31–49 (2013).
49. Arora, V. K. et al. Carbon–concentration and carbon–climate feedbacks in CMIP6 models and their comparison to CMIP5 models. *Biogeosciences* **17**, 4173–4222 (2020).
50. Wu, T. et al. Global carbon budgets simulated by the Beijing Climate Center Climate System Model for the last century. *J. Geophys. Res. Atmos.* **118**, 4326–4347 (2013).
51. Arora, V. K. et al. Carbon emission limits required to satisfy future representative concentration pathways of greenhouse gases. *Geophys. Res. Lett.* **38**, L05805 (2011).
52. Gent, P. R. et al. The community climate system model version 4. *J. Clim.* **24**, 4973–4991 (2011).
53. Collins, W. J. et al. Development and evaluation of an earth-system model—HadGEM2. *Geosci. Model Dev.* **4**, 1051–1075 (2011).
54. Dufresne, J.-L. et al. Climate change projections using the IPSL-CM5 earth system model: from CMIP3 to CMIP5. *Clim. Dyn.* **40**, 2123–2165 (2013).
55. Giorgetta, M. A. et al. Climate and carbon cycle changes from 1850 to 2100 in MPI-ESM simulations for the Coupled Model Intercomparison Project phase 5. *J. Adv. Model. Earth Syst.* **5**, 572–597 (2013).
56. Taylor, K. E., Stouffer, R. J. & Meehl, G. A. An overview of CMIP5 and the experiment design. *Bull. Am. Meteorol. Soc.* **93**, 485–498 (2012).
57. Joos, F. et al. Carbon dioxide and climate impulse response functions for the computation of greenhouse gas metrics: a multi-model analysis. *Atmos. Chem. Phys.* **13**, 2793–2825 (2013).

Acknowledgements

This study was supported by the National Natural Science Foundation of China (41988101 and 42001089). CH acknowledges the NERC National Capability Fund made to the UKCEH.

Author contributions

S.P. designed the research; M.H. performed analysis; M.H., S.P., and C.H. drafted the paper; M.H., S.P., C.H., H.X., X.W., A.B., J.C., and T.G. contributed to the interpretation of the results and to the text.

Competing interests

The authors declare no competing interests.

Additional information

Supplementary information The online version contains supplementary material available at <https://doi.org/10.1038/s43247-022-00489-4>.

Correspondence and requests for materials should be addressed to Shilong Piao.

Peer review information *Communications Earth & Environment* thanks Sujay Kumar and the other, anonymous, reviewer(s) for their contribution to the peer review of this work. Primary Handling Editors: Nadine Mengis and Clare Davis.

Reprints and permission information is available at <http://www.nature.com/reprints>

Publisher's note Springer Nature remains neutral with regard to jurisdictional claims in published maps and institutional affiliations.



Open Access This article is licensed under a Creative Commons Attribution 4.0 International License, which permits use, sharing, adaptation, distribution and reproduction in any medium or format, as long as you give appropriate credit to the original author(s) and the source, provide a link to the Creative Commons license, and indicate if changes were made. The images or other third party material in this article are included in the article's Creative Commons license, unless indicated otherwise in a credit line to the material. If material is not included in the article's Creative Commons license and your intended use is not permitted by statutory regulation or exceeds the permitted use, you will need to obtain permission directly from the copyright holder. To view a copy of this license, visit <http://creativecommons.org/licenses/by/4.0/>.

© The Author(s) 2022